Energy & Environmental Science

ROYAL SOCIETY OF CHEMISTRY

PAPER

View Article Online
View Journal | View Issue

Cite this: *Energy Environ. Sci.*, 2024, **17**, 8866

Self-healing polymer dielectric exhibiting ultrahigh capacitive energy storage performance at 250 °C†

Wenhan Xu, ‡ Fei Yang,‡ Guodong Zhao, Shixian Zhang, Guanchun Rui, Muchen Zhao, Lingling Liu, Long-Qing Chen and Qing Wang *

Received 18th August 2024,
Accepted 15th October 2024

DOI: 10.1039/d4ee03705g

rsc.li/ees

Polymer dielectrics capable of operating at elevated temperatures are essential components in advanced electronics and electrical power systems. However, dielectric polymers generally display significantly deteriorated capacitive performance at high temperatures because of exponential growth of electrical conduction. Here we design and prepare the cross-linked copolymers with interrupted translational symmetry and the use of local disorder-induced electron localization (*i.e.*, Anderson localization) to impede electrical conduction of the copolymers. Consequently, the copolymer exhibits state-of-the-art discharged energy density of 3.5 J cm^{-3} with a charge–discharge efficiency of 90% at 250 °C. The copolymer also displays much more stable capacitive energy storage performance in the temperature range of 25 to 250 °C compared to existing dielectric polymers. With the demonstrated breakdown self-healing ability and excellent cyclability of the copolymer, this work sheds a new light on the design of high-temperature high-energy-density polymer dielectrics.

Broader context

Polymers are the preferred materials for high-energy-density energy storage capacitors due to their high breakdown strength and facile processability. However, the performance of existing dielectric polymers is compromised under extreme conditions and fails to meet the growing demands in electric vehicles, aerospace systems, and power grids. In this work, we utilize the broken translational symmetry in the crosslinked copolymers to reduce leakage current and conduction loss, leading to the dielectric polymers with excellent energy densities and stable capacitive performance from room temperature to 250 °C. We further describe the self-healing ability of the polymers that can restore dielectric properties and capacitive performance after electrical breakdown. This approach establishes a new paradigm for the structural design of polymer dielectrics to address the critical needs of high-temperature electrical energy storage.

1. Introduction

In line with the continuous progress of electrification and the evolving requirements of the internet of things (IoT), dielectric capacitors, which are fundamental components in advanced electrical power systems and electronic devices, are demanded to exhibit reliable functionality across a diverse spectrum of operational scenarios.[1–7] Polymer film capacitors, widely chosen for their outstanding breakdown strength, unique self-healing capabilities, ease of processing and scalability, confront several challenges when deployed in extreme environments.[8–13] Biaxially oriented polyethylene films (BOPP), recognized as the best commercially available polymer dielectric, typically operate at temperatures below ~85 °C. When temperature is above 85 °C, they have a 30–50% voltage derating due to deterioration in the breakdown strength and lifetime of the films.[4,14] To enable the use of BOPP at high temperatures, the additional cooling units are brought in, *e.g.*, electric vehicles, to reduce the capacitor temperature, which unfortunately adds complexity to the system and decreases fuel efficiency. In the fields such as oil and gas exploration and aerospace systems, where spatial constraints hinder the integration of refrigeration systems for capacitors, there is a pressing demand for the capacitors constructed with high-temperature dielectrics that are capable of maintaining consistent performance across a broad temperature range (Table S1, ESI†).[15,16]

High-temperature polymer dielectrics have been extensively developed over the last decade to meet the urgent needs, in which electrical conduction is identified as the main loss

Department of Materials Science and Engineering, The Pennsylvania State University, University Park, Pennsylvania 16802, USA. E-mail: wang@matse.psu.edu

† Electronic supplementary information (ESI) available. See DOI: https://doi.org/10.1039/d4ee03705g

‡ These authors contributed equally.

mechanism.[1,3,16–24] The exponential increase in electrical conduction with the applied electric fields and temperatures leads to substantially decreased discharge energy density (U_d) and charge–discharge efficiency (η) of polymer dielectrics compared to those obtained at ambient temperature.[1,3] U_d directly impacts the size, compactness and modernization of electrical power systems, while η is indicative of dielectric loss and affects lifetime and reliability of dielectric materials during continuous operation. The addition of inorganic fillers with wide bandgaps, such as boron nitride,[2,25] alumina,[15,26] and silicon dioxide,[27,28] which can effectively impede the electrical conduction, has been utilized in the creation of high-temperature dielectric polymer composites. Similarly, high-temperature dielectric polymers have been designed based on the incorporation of high-electron-affinity units into high-glass-transition (T_g) polymers and the modulation of bandgaps of the aromatic polymers.[29–32] While these approaches are effectively in improving U_d and η at elevated temperatures, most of the current high-temperature polymer dielectric still suffer from relatively large variations of the capacitive performance over temperature. For instance, the best high-temperature polymer films such as polyetherimides (PEI) and fluorene polyester (FPE), their η decreases $>50\%$ with increasing temperature from 25 °C to 200 °C. Moreover, most research on high-temperature dielectric polymers is focused on temperatures below 200 °C, and expanding the operating temperature range to higher temperature of dielectric polymer remains a challenge. In addition to the parameters such as U_d, η and Weibull breakdown strength (E_b), self-healing capability, *i.e.*, the ability of a metallized capacitor to clear a fault area and restore its capacitance prior to catastrophic failure, is a key metric for evaluating the reliability of metallized film capacitors and assessing the suitability of new polymer dielectrics for practical applications. However, because of high ratios of carbon atoms in the aromatic structures such as PEI, polyimides, and poly(ether ether ketone), only a few aromatic polymers have been shown the breakdown self-healing ability.[33,34]

In this work, we design and synthesize the cross-linked copolymer based on divinyltetramethyldisiloxane-bis(benzocyclobutene) (*c*BCB) as high-temperature dielectrics. In particular, by introducing methanesulfonic acid modified norbornene (*N*-4-aminophenyl sulfonylmethyl-norbornene imide, SNI) to break the translational symmetry of the polymer network, the local disorder-induced electron localization (*i.e.*, Anderson localization), for the first time, is applied to reduce the hopping distance and electrical conduction of the polymer dielectrics at elevated temperatures and high applied fields. Remarkable capacitive energy storage performance, *i.e.*, an U_d of 3.5 J cm^{-3} at 250 °C and stable $\eta > 90\%$ at an applied field of 475 MV m^{-1} in the temperature ranging from 25–250 °C, has been demonstrated in the copolymer, which outperforms the current high-temperature polymer and polymer composite dielectrics. Moreover, U_e exhibits modest variation with temperature, with only −1.9% from 25 °C to 200 °C and −9.8% to 250 °C. The demonstration of self-healing ability and outstanding cyclic stability in the copolymer further suggests the promise of this structural design in the development of high-energy-density dielectric polymers for wide temperature range applications.

2. Result and discussion

2.1 Design of polymer dielectric with Anderson localization

The conduction model of the hopping motion of localized electrons with distribution function is the underlying mechanism responsible for the electric conduction of dielectrics. While this single-particle hopping model is similar to the one for mesoscopic transport behavior,[35] an effective strategy to reduce the conductivity in the field of the mesoscopic transport is to utilize the Anderson disorder localization, a fundamental phenomenon of the electric-conductivity reduction by local disorder as a consequence of the breaking of the translational symmetry.[35] To investigate the applicability of this effect in polymer dielectrics, we use tetra-functionality of BCB to prepare the cross-linked *c*BCB and also introduce a small amount of monofunctional SNI into the network as internal disorder sites (Fig. 1a and b). Topologically, this structure is equivalent to a two-dimensional single-particle hopping model within the field of the mesoscopic transport (shown in Fig. 1c and Fig. S1, ESI†),[35] in which the Hamiltonian H of electrons can be expressed as:

$$H = \sum_i U_i c_i^\dagger c_i + \sum_{\langle i,j \rangle} t_{ij} c_i^\dagger c_j \quad (1)$$

where $c_i^\dagger$ and c_i denote the creation and annihilation operators of electron at site i, respectively; $\langle i,j \rangle$ denotes that the summation is restricted to the nearest-neighbor sites with connection; t describes the hopping strength; U_i represents the on-site energy, and we set the on-site potential energy $U_i = U$ for disorder site and $U_i = 0$ for other sites.

The field of the mesoscopic transport concerns the electron transmission coefficient (T), which describes the probability of the transmitted electron to that of the incident electron, *i.e.*, the probability of electron tunneling/hopping through a potential barrier or well.

For the structure in Fig. 1c, we calculate T around a single local disorder within the framework of the Landauer–Buttiker approach,[35] and the numerical results are presented in Fig. 1d. For illustration, we first artificially set a four-link connection of the SNI (blue curve) into the cross-linked network. As seen from the figure, the increase in the difference of the on-site potential energies between disorder site and normal site from zero remarkably reduces transmission coefficient T no matter whether this difference is positive or negative. This is because for a positive energy difference, the hopping electrons need to cross a potential barrier with the possibility of the reflection/back-scattering whereas for a negative difference, the potential well due to the local disorder provides the possibility of the electron trapping. Both are detrimental to the electron transmission. We next consider the single-link connection of SNI. It is noted that there are two cases for the remaining link along and perpendicular to the transport direction. We therefore calculate the average of transmission coefficient T for both cases (yellow curve). As seen from the figure, a sharp anti-resonance of the transmission coefficient T emerges in the regime of negative U. This is because for single-link connection, the localized state due to a negative U on a local disorder has a

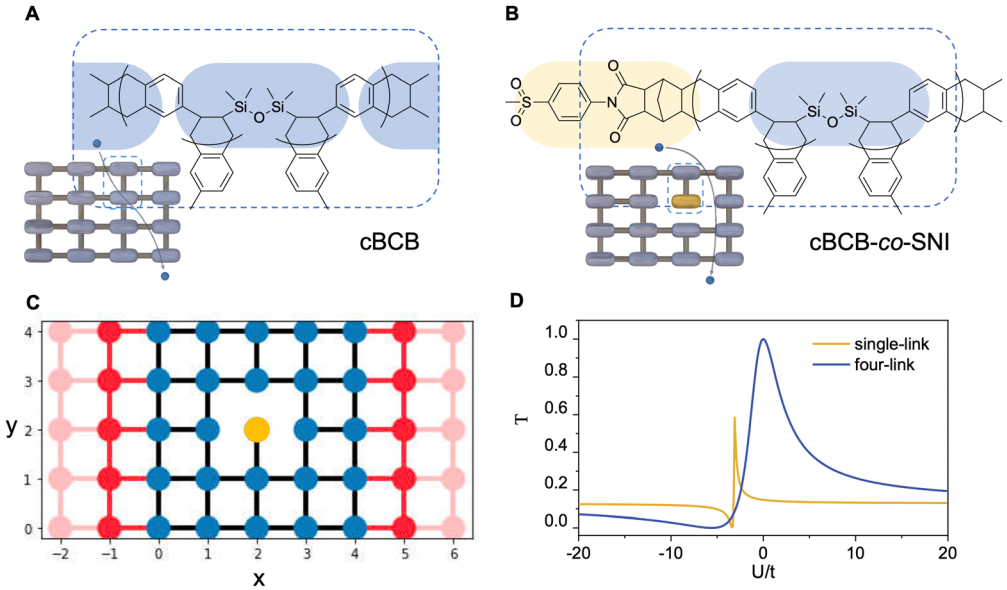

Fig. 1 Design and structures of high-temperature dielectric copolymers. (A) and (B) The chemical structure of *c*BCB and *c*BCB-*co*-SNI. Insets: Conduction models of the corresponding cross-linked networks. (C) Schematic of a two-dimensional single particle hopping model with tangent connection to the metal electrode (red part). The blue part denotes the cross-linked network formed by *c*BCB and the yellow part stands for the monofunctional monomer (SNI) which serves as an internal disorder site. (D) Calculated electron transmission coefficient *T vs.* on-site energy of the disorder for the single link with monofunctional monomer (yellow curve) and the tetrafunctional link (blue curve) involved in the cross-linked network.

strong localization character, and the existence of the strongly localized state provides the discrete channel to interfere with the conducting channel, leading to a characteristic, asymmetric line shape in the transmission spectroscopy, known as the Fano-type anti-resonance.[36,37] It is noted that, as a consequence of the single-link connection (*i.e.*, Fano effect), the peak of the electron transmission gets suppressed in comparison with the case for the four-link connection, which suppresses the localization character due to a stronger connection to the normal sites.

Consequently, for the structure shown in Fig. 1c, besides the on-site potential energy, the monofunctional monomer SNI brings an additional translational-symmetry breaking: a single-link connection to the cross-linked network, differing from the four-link one of *c*BCB. Both origins can lead to a remarkable reduction in transmission coefficient T. Moreover, as a consequence of the Anderson disorder localization *via* the unique translational-symmetry breaking by SNI, the resulted transmission coefficient T is very robust against structure distortion (*i.e.*, fluctuation of hopping or on-site energy on normal sites) and disturbance by external fields as well as thermal fluctuation, making this design highly feasible for high-temperature high-field dielectric applications.

2.2 Electrical and dielectric characteristics

The leakage current density of *c*BCB-*co*-SNI with different contents of SNI are measured at high temperatures. As shown in Fig. S2 and S3 (ESI†), *c*BCB-*co*-SNI with 5 mol% SNI consistently exhibits the lowest leakage current density and the smallest charge carrier hopping distance. The larger leakage current at >5 mol% SNI is attributable to higher conduction of SNI relative to that of *c*BCB. Fig. 2a compares the leakage current and resistivity of *c*BCB and *c*BCB-*co*-SNI (in which SNI constitutes 5 mol%, unless otherwise specified) measured at high temperatures as a function of the applied electric fields. Consistent with theoretical predictions, the leakage current of the copolymer film is found to be notably smaller compared to that of pristine *c*BCB. Specifically, at 200 MV m^{-1} and 200 °C, the leakage current is decreased more than an order of magnitude from 4.76×10^{-7} A cm^{-2} of *c*BCB to 3.96×10^{-8} A cm^{-2} of *c*BCB-*co*-SNI. Comparatively, state-of-the-art polymer dielectrics like PSBNP-*co*-$PTNI_{0.02}$ and *sc*-PEENA exhibit relatively higher leakage currents, reported as 5.56×10^{-8} A cm^{-2} and 2.42×10^{-7} A cm^{-2}, respectively, under the same condition.[1,32] At 200 MV m^{-1} and 250 °C, the copolymer shows an exceptionally low leakage current of only 1.94×10^{-7} A cm^{-2} which is the smallest leakage current reported so far in polymer and composite dielectrics.

Based on the hopping conduction equation,

$$J(E,T) = 2ne\lambda\nu \times \exp\left(-\frac{W_a}{K_B T}\right) \times \sinh(\lambda eE/2K_B T) \qquad (2)$$

J represents the conductivity and is determined by parameters such as carrier concentration (n), hopping distance (λ), attempt-to-escape frequency (ν), activation energy (W_a) in electron volts (eV) and charge of carriers (e). The excellent agreement between the fitting hyperbolic sine curve with eqn (2) and the experimental data, with coefficients of determination (R^2) ranging from 0.956 to 0.997, suggests that hopping serves as the predominant conduction mechanism in *c*BCB and the copolymer. Fitting the J–E data to the hopping conduction model reveals a hopping distance that escalates from 1.45 to 1.94 nm in pristine *c*BCB and from 0.82 to 1.60 nm in *c*BCB-*co*-SNI with

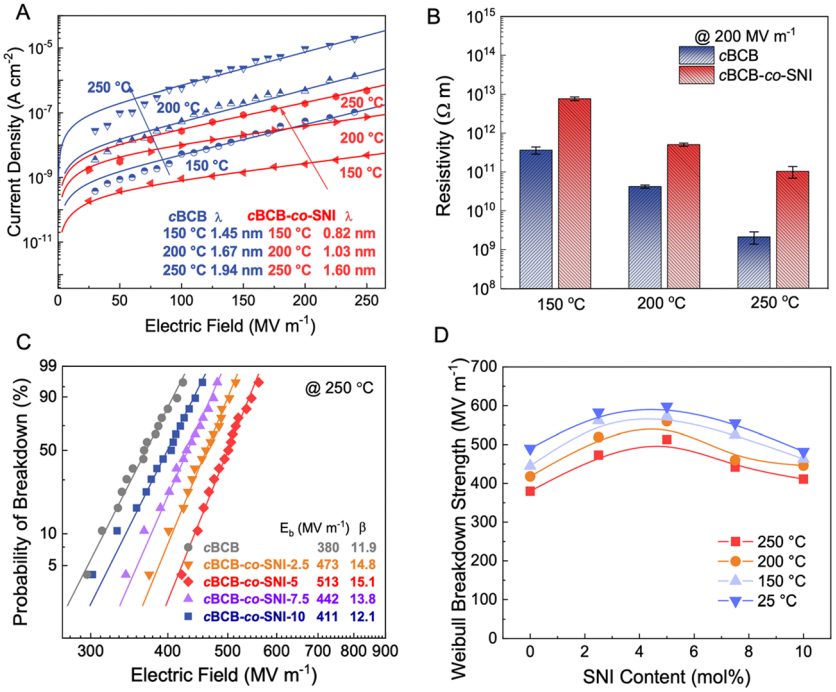

Fig. 2 Electrical properties and breakdown strength. (A) Electric field-dependent current density of *c*BCB and *c*BCB-*co*-SNI. (B) Comparison of electrical resistivity of *c*BCB and *c*BCB-*co*-SNI at various temperatures. (C) Weibull breakdown strength of *c*BCB and *c*BCB-*co*-SNI at 250 °C. (D) Composition-dependent Weibull breakdown strength of *c*BCB-*co*-SNI at different temperatures.

temperature rises from 150 to 250 °C (as shown in Fig. 2a and Fig. S3, ESI†). Variation in the hopping distance can be well explained by Anderson disorder localization. The hopping distance can be understood as the average movement distance of electrons within the material without being disturbed. It is proportional to the velocity of the electron v_e and the collision time of the electrons τ,

$$\lambda = v_e\tau \tag{3}$$

$$\frac{1}{\tau} = \frac{1}{\tau_{phonon}} + \frac{1}{\tau_{disorder}} \tag{4}$$

$1/\tau$ denotes the probability of electron collision per unit time. With the introduction of disorder sites, additional collision probabilities emerge within the system, augmenting the overall collision likelihood. Since the calculated transmission coefficient T describes the probability of electron hopping through the local disorder, the hopping distance around local disorder becomes $\lambda_{ad} = \lambda_0 T$,[38,39] where λ_0 represents the hopping distance without disorder. The calculated transmission coefficient T near the disorder site as shown in Fig. 1d consistently falls below 0.2 across various energy conditions. This indicates that λ_{ad} will be significantly smaller than λ_0, thus diminishing the macroscopic average λ of *c*BCB-*co*-SNI. This is also reflected in the increased resistivity of the polymers. As depicted in Fig. 2b and Fig. S4 (ESI†), the resistivity is increased from 3.6×10^{11} Ω m, 4.2×10^{10} Ω m and 2.1×10^{9} Ω m for pristine *c*BCB to 7.7×10^{12} Ω m, 5.1×10^{11} Ω m and 1.0×10^{11} Ω m for *c*BCB-*co*-SNI at temperatures of 150 °C, 200 °C, and 250 °C, respectively.

We also calculate the effect of the SNI ratio x in the copolymer on the conductivity. At finite but small x, one can apply the random phase approximation where the collision rate $1/\tau_{disorder}$ of electrons with disorder is proportional to the disorder concentration, *i.e.*, $1/\tau_{disorder} = x/\tau^0_{disorder}$ with $\tau^0_{disorder}$ being the collision time of electrons by single disorder. Then, considering the ratio *c*BCB $(1 - x)$, from eqn (2)–(4), one finds that the electric conductance at small x reads

$$\sigma = (1 - x)\sigma_{cBCB}\frac{1}{1 + \gamma x} \tag{5}$$

where $\gamma = \tau_{phonon}/\tau^0_{disorder}$ and σ_{cBCB} denotes the conductivity of the pristine *c*BCB. Consequently, with the increase in x from zero, σ decreases from σ_{cBCB} as it should be. Particularly, with the conductivity $\sigma = 0.65\sigma_{cBCB}$ at $x = 2.5\%$, 100 MV m^{-1} and 150 °C, one finds $\gamma \approx 20$. As for large x, the intrinsic conducting charater of SNI dominates and *c*BCB serves as disorder to SNI. In this situation, similar to eqn (6), one finds approximately

$$\sigma = \sigma_{SNI}\frac{x}{1 + \gamma'(1 - x)} \tag{6}$$

where σ_{SNI} stands for the conductivity of pristine SNI. Then, at large x, σ increases with the increase in x until $\sigma = \sigma_{SNI}$ at $x = 1$ as it should be. With $\sigma_{SNI} \approx 25\sigma_{cBCB}$, for $\gamma' = 0.2$, one finds $\sigma \sim 2.2\sigma_{cBCB}$ at $x = 10\%$ and $\sigma \sim 1.58$ at $x = 7.5\%$, close to the corresponding experimental values $\sigma = 2.5\sigma_{cBCB}$ at $x = 10\%$ and $\sigma = 1.47\sigma_{cBCB}$ at $x = 7.5\%$, 100 MV m^{-1} and 150 °C. In the regime between small and large x, there is a competion between two mechanisms in eqn (5) and (6) above. Therefore, the conductivity in principle reaches its minimum when two mechanisms

are comparable to each other [*i.e.*, $\sigma_{cBCB}(1-x)/(1+\gamma x) \sim \sigma_{SNI}x/(1+\gamma'(1-x))$] where $x_m \approx 3\%$, close to the value $x_m \approx 5\%$ of the experimental results.

The dielectric spectra of *c*BCB and *c*BCB-*co*-SNI are presented in Fig. S5 and S6 (ESI†). It is evident that the dielectric constant of the copolymers increases with the SNI content, *e.g.*, from 2.76 of *c*BCB to 3.10 of *c*BCB-*co*-SNI, while the dissipation loss essentially remains unchanged. The dielectric constant and dissipation factor of *c*BCB and *c*BCB-*co*-SNI are highly stable over a wide range of temperature from 25–250 °C and frequency from 10^2–10^6 Hz.

2.3 Capacitive energy storage performance

We examine the breakdown strength of the dielectric films utilizing Weibull statistics at various temperatures as summarized in Fig. 2c, d and Fig. S7 (ESI†). The cumulative probability of electric breakdown $P(E)$ is represented by the equation:

$$P(E) = 1 - \exp(-E/E_b)^{\beta} \quad (7)$$

where E denotes the electric field, E_b signifies the characteristic breakdown strength corresponding to a cumulative failure probability of 63.2%, and β represents the shape parameter. As shown in Fig. 2c, the significant improvement of E_b with the incorporation of SNI is clearly demonstrated, *e.g.*, from 380 MV m^{-1} of *c*BCB to 513 MV m^{-1} of *c*BCB-SNI-5 at 250 °C, which surpasses those of the current high temperature dielectric polymers such as PI-CF_3-iso[29] with an E_b of 458 MV m^{-1} at 250 °C. Consistent to the electrical resistivity results, E_b of the copolymers is maximized at 5 mol% SNI at temperatures ranging from 25 to 250 °C.

Fig. 3a and b compare the U_d and η of *c*BCB-*co*-SNI with those of the current high-performance dielectric polymers, including *c*BCB, BOPP, PEI, FPE, and PI-CF_3-iso,[29] measured at 250 °C. *c*BCB-*co*-SNI delivers the maximal U_d of 3.8 J cm^{-3} compared with 1.8 J cm^{-3} of *c*BCB, 2.7 J cm^{-3} of PI-CF_3-iso, 0.3 J cm^{-3} of FPE and 0.2 J cm^{-3} of PI at 250 °C. The best U_d achieved in *c*BCB-*co*-SNI is apparently benefited from its much-reduced conduction and higher E_b which is attributed to its unique crosslinked structure with local disorder-induced electron localization. Indeed, the copolymer displays a superior η of 86.4% to 61% of PI-CF_3-iso and all other high-temperature dielectric polymers at 250 °C and 500 MV m^{-1}. It is noteworthy that *c*BCB-*co*-SNI exhibits highly stable η of over 90% up to the applied field of 475 MV m^{-1} at 250 °C. The achieved U_d of 3.5 J cm^{-3} at $\eta \geq 90\%$ also represents the state-of-the-art in dielectric polymers measured at 250 °C, improving the current performance record by over 50%. Specifically, we increased the maximum energy storage density from 2.2 J cm^{-3} of PI-CF_3-iso to 3.5 J cm^{-3} of *c*BCB-*co*-SNI at over 90% efficiency (as shown in Fig. S8, ESI†). The *P*–*E* loops, along with U_d and η, of the copolymers with different compositions, are presented in Fig. S9 and S10 (ESI†). *c*BCB-*co*-SNI-5 exhibits the best overall capacitive performance.

We further compare the U_d and η of the copolymer with the current high-temperature polymer dielectrics measured 500 MV m^{-1} as a function of temperature to assess their temperature stability. As summarized in Fig. 3c and d, *c*BCB-*co*-SNI clearly has much better stability of U_d and η, *i.e.*, ΔU_d of −9.8% and $\Delta\eta$ of −10.1% compared to ΔU_d of −26.5% and $\Delta\eta$ of −35.4% of PI-CF_3-iso with increasing temperature from 25 to

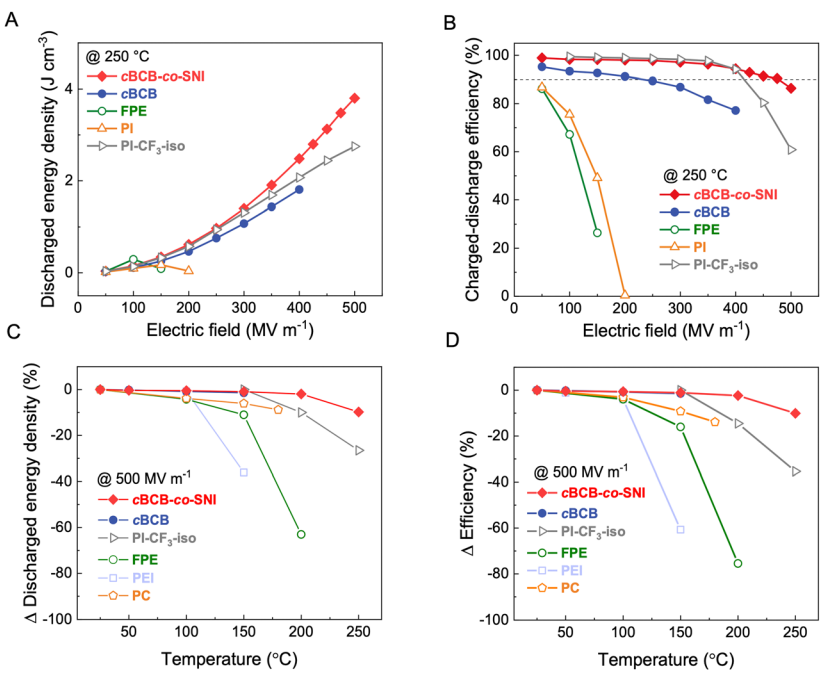

Fig. 3 Capacitive energy storage performance. (A) Discharged energy density and (B) charge–discharge efficiency of *c*BCB-*co*-SNI, PI-CF_3-iso[29] and other high-temperature dielectric polymers as a function of the applied electric field at 250 °C. (C) and (D) Change in (C) discharged energy density and (D) charge–discharge efficiency of the dielectric polymers as a function of temperature measured at 500 MV m^{-1}.

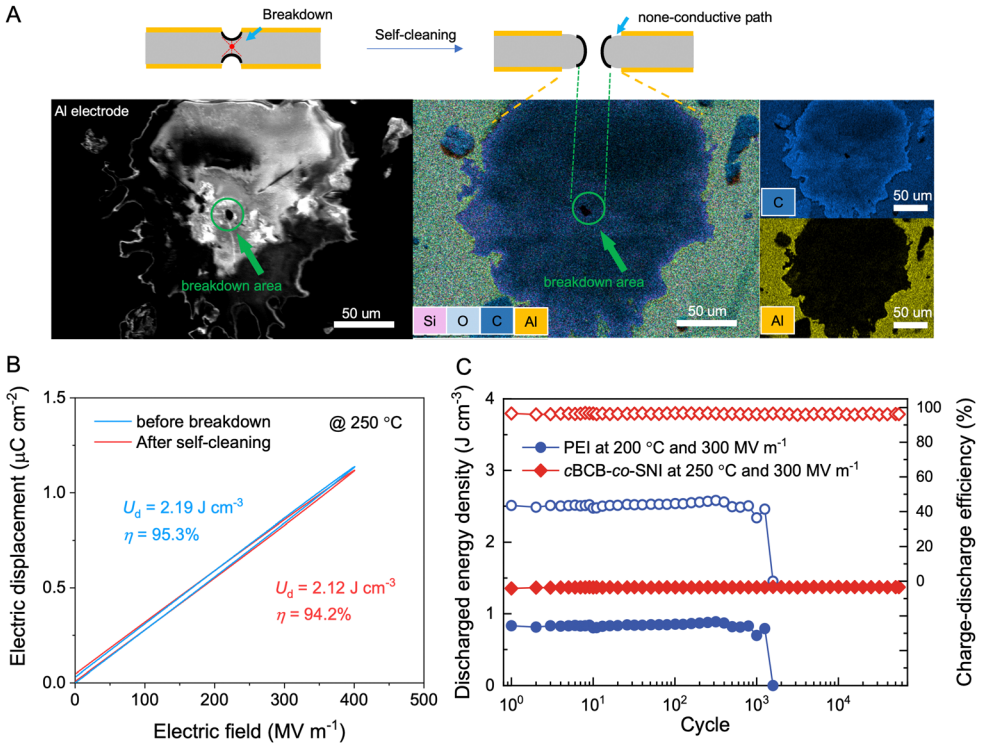

Fig. 4 Self-healing and cyclic stability. (A) SEM image and EDS analysis of *c*BCB-*co*-SNI film after electrical breakdown. Scale bars, 50 μm. (B) Electric displacement–electric field loops of *c*BCB-*co*-SNI before breakdown and after self-healing at 250 °C. (C) Cyclic performance of *c*BCB-*co*-SNI and PEI at elevated temperatures.

250 °C and ΔU_d of −11% and $\Delta\eta$ of −16% observed in FPE in the temperature range from 25 to 150 °C, which is again attributed to the fact that the increase of the conductivity of *c*BCB-*co*-SNI with temperature is much less pronounced.

2.4 Self-healing ability and cyclability

While the theoretical link between chemical composition and the self-healing capability of dielectric polymers remains elusive, empirical observations suggest that, for polymers with a general formula of $C_\alpha H_\beta O_\gamma N_\delta S_\theta$, a low ratio of $(\alpha+\delta+\theta)$ to $(\beta+\gamma)$ usually correlates well with potential for the self-healing ability. Interestingly, *c*BCB-*co*-SNI has a ratio of ∼0.72 that is much lower than PSBNP-*co*-PTNI$_{0.02}$ of 0.97[1] and other high-temperature polymer dielectrics such as PEI (1.3), PI (1.6), and PET (0.83). The scanning electron microscopy/energy dispersive X-ray spectroscopy (SEM EDS) analysis of the *c*BCB-*co*-SNI film, depicted in Fig. 4a, reveals the vaporization of the electrode in the area where dielectric breakdown occurs. The destruction of the electrodes during the so-called self-cleaning process allows the spontaneous extinction of a local electrical arc and thus would prevent catastrophic failure for continuing the operation of the capacitor films. The dielectric constant and dissipation factor of the films show no significant variation before and after breakdown, indicating no conductive pathway formation (Fig. S16, ESI†). Consequently, as shown in Fig. 4b, minimal loss in the U_d and η measured at 400 MV m^{-1} and 250 °C is found in the dielectric films after self-cleaning.

Fig. 4c compares the cyclic performance of *c*BCB-*co*-SNI to that of PEI under an applied field of 300 MV m^{-1}. In contrast to commercial capacitor-grade PEI films that fail after less than 10 000 cycles at 200 °C, the *c*BCB-*co*-SNI film exhibits stable U_d and η up to 50 000 cycles at 250 °C. Curiously, the excellent stability of the copolymer cannot be credited to its mechanical properties since PEI has much greater mechanical strength (*i.e.*, Young's modulus of 1.1 GPa at 200 °C) than the copolymer with the Young's modulus of 0.49 GPa at 200 °C. On the other hand, at an applied field of 300 MV m^{-1}, the copolymer has remarkably lower conduction loss (*i.e.*, 2.9% at 250 °C) compared to PEI (6.6% at 150 °C and 56.4% at 200 °C). Therefore, it can be assumed that much less Joule heat resulting from lower loss in the copolymer is highly beneficial to long-term stability of dielectric films.

3. Conclusions

We strategically introduce monofunctional monomers to disrupt the translational symmetry of the cross-linked polymer and leverage the Anderson localization effect to effectively hinder the electrical conduction of the polymers at high electric fields and elevated temperatures. This design principle is different from the current approaches to high-temperature dielectric polymers. As a consequence of radically reduced conductivity resulting from the Anderson localization, the copolymer reported in this work displays outstanding U_d and

η at 250 °C, far exceeding the current polymer and composite dielectrics. More impressively, η of over 90% is maintained up to the applied field of 475 MV m^{-1} at 250 °C. The copolymer also exhibits significantly more stable capacitive energy storage performance over a wide temperature range from 25 to 250 °C than the current polymer and composite dielectrics. In addition, breakdown self-healing ability and excellent cyclability have been demonstrated in the copolymer. This work successfully improves the effective operating temperature of dielectric polymers from 200 to 250 °C and opens a new avenue for high-temperature dielectric polymers for their potential applications in electronics and power systems under extreme conditions.

Author contributions

Q. W. and W. X. conceived the idea. Q. W. and W. X. designed the experiments. W. X. and M. Z. conducted polymer synthesis. W. X. and L. L. prepared device samples for measurements. W. X., S. Z., and G. R. carried out electrical, thermal and optical measurements under the supervision of Q. W. F. Y. and G. Z. performed all simulations and theoretical part under the supervision of L. C. W. X. carried out SEM-EDS studies. W. X., S. Z., L. L., M. Z., G. R., and F. Y. analysed the data. Q. W., W. X., and F. Y. wrote the manuscript all authors discussed the results and provided inputs to the manuscript.

Data availability

The data supporting this article have been included as part of the ESI.†

Conflicts of interest

The authors declare no competing interests.

Acknowledgements

This research was supported by the US Office of Naval Research (N000142312267). The theoretical analysis based on the Anderson Location Model was supported by as part of the Computational Materials Sciences Program funded by the U.S. Department of Energy, Office of Science, Basic Energy Sciences, under Award No. DE-SC0020145 (F. Y. and L. Q. C.). L. Q. C. also acknowledges the support by the Hamer Foundation through the Hamer Professorship.

Notes and references

1 J. Chen, Y. Zhou, X. Huang, C. Yu, D. Han, A. Wang, Y. Zhu, K. Shi, Q. Kang, P. Li, P. Jiang, X. Qian, H. Bao, S. Li, G. Wu, X. Zhu and Q. Wang, *Nature*, 2023, **615**, 62–66.
2 Q. Li, L. Chen, M. R. Gadinski, S. Zhang, G. Zhang, H. U. Li, E. Iagodkine, A. Haque, L.-Q. Chen, T. N. Jackson and Q. Wang, *Nature*, 2015, **523**, 576–579.
3 J. Pei, L. Yin, S. Zhong and Z. Dang, *Adv. Mater.*, 2023, **35**, 2203623.
4 D. Tan, L. Zhang, Q. Chen and P. Irwin, *J. Electron. Mater.*, 2014, **43**, 4569–4575.
5 A. A. Deshmukh, C. Wu, O. Yassin, A. Mishra, L. Chen, A. Alamri, Z. Li, J. Zhou, Z. Mutlu, M. Sotzing, P. Rajak, S. Shukla, J. Vellek, M. Arab Baferani, M. Cakmak, P. Vashishta, R. Ramprasad, Y. Cao and G. Sotzing, *Energy Environ. Sci.*, 2022, **15**, 1307–1314.
6 G. Wang, Z. Lu, Y. Li, L. Li, H. Ji, A. Feteira, D. Zhou, D. Wang, S. Zhang and I. M. Reaney, *Chem. Rev.*, 2021, **121**, 6124–6172.
7 X. Wu, A. Karlin, V. Beilin, G. E. Shter, G. S. Grader, Y. Ivry, S. Lin and D. Q. Tan, *Adv. Mater.*, 2024, 2401597.
8 J. Chen, Y. Wang, H. Li, H. Han, X. Liao, R. Sun, X. Huang and M. Xie, *Chem. Mater.*, 2018, **30**, 1102–1112.
9 X. Li, B. Liu and J. Wang, *et al.*, *Nat. Commun.*, 2024, **15**, 6655.
10 B. Chu, X. Zhou, K. Ren, B. Neese, M. Lin, Q. Wang, F. Bauer and Q. M. Zhang, *Science*, 2006, **313**, 334–336.
11 J. Wei and L. Zhu, *Prog. Polym. Sci.*, 2020, **106**, 101254.
12 H. Li, B. S. Chang, H. Kim, Z. Xie, A. Lainé, L. Ma, T. Xu, C. Yang, J. Kwon, S. W. Shelton, L. M. Klivansky, V. Altoé, B. Gao, A. M. Schwartzberg, Z. Peng, R. O. Ritchie, T. Xu, M. Salmeron, R. Ruiz, K. B. Sharpless, P. Wu and Y. Liu, *Joule*, 2023, **7**, 95–111.
13 X. Wu, X. Chen, Q. M. Zhang and D. Q. Tan, *Energy Storage Mater.*, 2022, **44**, 29–47.
14 M. Rabuffi and G. Picci, *IEEE Trans. Plasma Sci.*, 2002, **30**, 1939–1942.
15 T. Zhang, X. Chen, Y. Thakur, B. Lu, Q. Zhang, J. Runt and Q. M. Zhang, *Sci. Adv.*, 2020, **6**, eaax6622.
16 Z. Zhang, D. H. Wang, M. H. Litt, L.-S. Tan and L. Zhu, *Angew. Chem.*, 2018, **130**, 1544–1547.
17 Y. Zhou, Y. Zhu, W. Xu and Q. Wang, *Adv. Energy Mater.*, 2023, **13**, 2203961.
18 C. Zhou, W. Xu, B. Zhang, Y. Zhang, C. Shen, Q. Xu, X. Liu, F. Bertram, J. Bernholc, Z. Jiang, Y. Shang and H. Zhang, *Chem. Mater.*, 2022, **34**, 2333–2341.
19 A. Alamri, C. Wu, A. Mishra, L. Chen, Z. Li, A. Deshmukh, J. Zhou, O. Yassin, R. Ramprasad, P. Vashishta, Y. Cao and G. Sotzing, *Chem. Mater.*, 2022, **34**, 6553–6558.
20 J. Dong, R. Hu, X. Xu, J. Chen, Y. Niu, F. Wang, J. Hao, K. Wu, Q. Wang and H. Wang, *Adv. Funct. Mater.*, 2021, **31**, 2102644.
21 Z. Dai, Z. Bao, S. Ding, C. Liu, H. Sun, H. Wang, X. Zhou, Y. Wang, Y. Yin and X. Li, *Adv. Mater.*, 2022, **34**, 2101976.
22 M. Yang, H. Li, J. Wang, W. Shi, Q. Zhang, H. Xing, W. Ren, B. Sun, M. Guo, E. Xu, N. Sun, L. Zhou, Y. Xiao, M. Zhang, Z. Li, J. Pan, J. Jiang, Z. Shen, X. Li, L. Gu, C.-W. Nan, X. Wang and Y. Shen, *Nat. Energy*, 2024, **9**, 143–153.
23 H. Li, E. Vargo, Z. Xie, L. Ma, P. F. Pieters, S. W. Shelton, A. P. Alivisatos, T. Xu and Y. Liu, *Adv. Mater.*, 2024, 2401954.
24 M. Dai, J. Sun and Q. Fang, *Mater. Today Sustainability*, 2023, **24**, 100557.
25 A. Azizi, M. R. Gadinski, Q. Li, M. A. AlSaud, J. Wang, Y. Wang, B. Wang, F. Liu, L.-Q. Chen, N. Alem and Q. Wang, *Adv. Mater.*, 2017, **29**, 1701864.

26 H. Li, D. Ai, L. Ren, B. Yao, Z. Han, Z. Shen, J. Wang, L.-Q. Chen and Q. Wang, *Adv. Mater.*, 2019, **31**, 1900875.
27 Y. Zhou, Q. Li, B. Dang, Y. Yang, T. Shao, H. Li, J. Hu, R. Zeng, J. He and Q. Wang, *Adv. Mater.*, 2018, **30**, 1805672.
28 G. Rui, J. (Jerry) Bernholc, S. Zhang and Q. Zhang, *Adv. Mater.*, 2024, 2311739.
29 R. Wang, Y. Zhu, J. Fu, M. Yang, Z. Ran, J. Li, M. Li, J. Hu, J. He and Q. Li, *Nat. Commun.*, 2023, **14**, 2406.
30 Z. Ran, R. Wang, J. Fu, M. Yang, M. Li, J. Hu, J. He and Q. Li, *Adv. Mater.*, 2023, **35**, 2303849.
31 H. Li, B. S. Chang, H. Kim, Z. Xie, A. Lainé, L. Ma, T. Xu, C. Yang, J. Kwon, S. W. Shelton, L. M. Klivansky, V. Altoé, B. Gao, A. M. Schwartzberg, Z. Peng, R. O. Ritchie, T. Xu, M. Salmeron, R. Ruiz, K. B. Sharpless, P. Wu and Y. Liu, *Joule*, 2023, **7**, 95–111.
32 W. Xu, C. Zhou, W. Ji, Y. Zhang, F. Bertram, Z. Jiang, Y. Shang, H. Zhang and C. Shen, *Angew. Chem., Int. Ed.*, 2024, e202319766.
33 J. S. Ho and S. G. Greenbaum, *ACS Appl. Mater. Interfaces*, 2018, **10**, 29189–29218.
34 H. Li, Y. Zhou, Y. Liu, L. Li, Y. Liu and Q. Wang, *Chem. Soc. Rev.*, 2021, **50**, 6369–6400.
35 S. Datta, *Electronic Transport in Mesoscopic Systems*, Cambridge University Press, Cambridge, 1995.
36 U. Fano, *Phys. Rev.*, 1961, **124**, 1866–1878.
37 A. E. Miroshnichenko, S. Flach and Y. S. Kivshar, *Rev. Mod. Phys.*, 2010, **82**, 2257–2298.
38 V. Ambegaokar, B. I. Halperin and J. S. Langer, *Phys. Rev. B: Solid State*, 1971, **4**, 2612–2620.
39 P. Coleman, P. W. Anderson and T. V. Ramakrishnan, *Phys. Rev. Lett.*, 1985, **55**, 414–417.